Postharvest Biology and Technology 121 (2016) 71–77

Contents lists available at ScienceDirect

Postharvest Biology and Technology

journal homepage: www.elsevier.com/locate/postharvbio

Monitoring attenuation and the elastic properties of an apple with laser ultrasound

Sam Hitchman[a,b,*], Kasper van Wijk[a,b], Zoe Davidson[a,b]

[a] Dodd Walls Centre for Photonic and Quantum Technologies, New Zealand
[b] The Physical Acoustics Lab, Department of Physics, University of Auckland, New Zealand

ARTICLE INFO

Article history:
Received 19 April 2016
Received in revised form 23 June 2016
Accepted 10 July 2016

Keywords:
Acoustic monitoring
Elastic properties
Apple texture
Laser ultrasound
Attenuation

ABSTRACT

The firmness of an apple is a commonly used indicator of quality and maturity during sorting and cold storage. Its dependence on the elastic properties means that vibration resonance tests are favored over other – often destructive – tests. We present a novel non-destructive and non-contacting method using laser-generated and laser-detected elastic waves to infer the elastic modulus and Poisson's ratio of an apple from the velocity of surface and body waves. In addition, we analyze the attenuation of these waves. Although the elastic and anelastic properties all decay with age, attenuation is the most sensitive to changes in ripeness of the apple.

1. Introduction

Optical absorption spectrum and scattering of light in fruit have been used to non-destructively infer fruit soluble solid content (Peng and Lu, 2007) and texture (Lu and Peng, 2006; Huang and Lu, 2010). Several other methods test the firmness of fruit, both at the point of harvest and periodically in cold storage, as an indicator of fruit quality. Magness–Taylor (MT) pressure tests involve a small cylindrical rod being pushed into the fruit until permanent deformation occurs. The force required to deform fruit flesh is used as a quantitative firmness measurement (Magness and Taylor, 1925). The MT index is often considered the gold standard of quantitative firmness testing techniques, and the most widely used (Abbott et al., 1992). An apple's elastic properties can also be measured by compressing cylindrical sections of apple flesh and measuring the stress–strain relationship (Khan and Vincent, 1993; Varela et al., 2007). In addition to these destructive methods, non-destructive tests exist which measure the frequency of an apple's vibrational modes, which can be used to infer elastic properties (Cooke and Rand, 1973; Abbott et al., 1968; Lu and Abbott, 1996; Zhang et al., 2014). The Firmness Index (FI) combines measurements of the fundamental resonant vibration mode f_l, and mass m in such a way that it correlates with MT results:

$$FI = f_l^2 m^{2/3}. \quad (1)$$

The frequency of the resonant mode is dependent on the shape, size and elastic constants of the fruit (Lu and Abbott, 1996; Cooke and Rand, 1973). Chen and DeBaerdemaeker (1993) derived that for a sphere FI is proportional to the elastic modulus E:

$$FI = \left[\frac{(1-\nu)}{\rho^{1/3}(6\pi^2)^{2/3}(1+\nu)(1-2\nu)}\right]\left(\frac{2\pi f_l R}{v_P}\right)^2 E, \quad (2)$$

where R is the radius, ν the Poisson's ratio, ρ the density, and v_P the compressional wave speed of the sphere.

Duprat et al. (1997) report a correlation coefficient of 0.8391 between the FI and MT experiments on apples in cold storage over a number of months. Resonance tests are favored over pressure tests, as the former is non-destructive and sample the entire apple (Duprat et al., 1997; Abbott et al., 1992). We present elastic wavefield measurements and a quantitative analysis of an intact apple using an optical system, which is non-contacting and non-destructive. Laser ultrasonic techniques (Scruby and Drain, 1990; Blum et al., 2010; Hitchman et al., 2015) are used to generate and detect the elastic waves in the apple, overcoming many of the limitations associated contacting resonant experiments. A contacting system with an impulse hammer and non-contacting microphones in fixed positions around an apple has previously been used to characterize fruit (Chen et al., 1996), and ultrasound has been used to estimate the elastic modulus of watermelon (Ikeda et al., 2015), for

* Corresponding author.
E-mail address: shit014@aucklanduni.ac.nz (S. Hitchman).

http://dx.doi.org/10.1016/j.postharvbio.2016.07.006
0925-5214/

example. To quantitatively estimate the apple's elastic properties, we use a high-energy pulsed laser to generate elastic waves in an apple via thermoelastic expansion, and a laser Doppler interferometer to detect elastic waves. Such a system has been successfully used in geophysics [e.g., Adam et al., 2014; Blum et al., 2013] and medical imaging [e.g., Johnson et al., 2014], but has not previously been applied to fruit.

2. Materials and methods

2.1. Wave propagation and modes

Elastic wave propagation is a well established method to estimate the elastic properties of solids. One classic application is seismology, where elastic waves generated by earthquakes or man-made explosions are used to infer the elastic properties of the Earth [e.g., Aki and Richards, 2002]. For an isotropic medium, two elastic constants and the density define elastic wave propagation. Often such media are represented by the elastic or Young's modulus, E, and the Poisson's ratio, ν, where the former describes the amount of strain when stress is applied in the same dimension, while the latter is the ratio between the strain in orthogonal directions from stress [e.g., Stein and Wysession, 2009].

2.1.1. Time domain: propagating waves

First, we quantitatively estimate E and ν from the propagation speeds of primary waves (also called compressional waves, or P-waves), secondary waves (shear, or S-waves), and surface waves. P- and S-waves are body waves that travel through the apple flesh. The S-wave velocity v_S, and P-wave velocity v_P in an isotropic medium, together with the density ρ uniquely define the elastic moduli:

$$E = v_S^2\rho\left(\frac{(v_P^2/v_S^2)-2}{(v_P^2/v_S^2)-1}+2\right), \quad \nu = \frac{1}{2}\left(\frac{(v_P^2/v_S^2)-2}{(v_P^2/v_S^2)-1}\right). \tag{3}$$

Conversely, Rayleigh waves are surface waves with a combination of longitudinal and transverse particle motion (Stein and Wysession, 2009). As surface-wave geometric spreading happens over a surface – rather than over a volume for body waves – Rayleigh waves are often dominant features in the recorded wave field. By solving the boundary conditions for an elastic wave trapped at a surface the Rayleigh wave velocity, v_R, can be related to v_S and v_P such that the following condition is satisfied (Rayleigh, 1885; Stein and Wysession, 2009):

$$\left(2-\frac{v_R^2}{v_S^2}\right)^2 + 4\sqrt{\frac{v_R^2}{v_S^2}-1}\sqrt{\frac{v_R^2}{v_P^2}-1} = 0, \tag{4}$$

with the requirement that $0 < v_R < v_S$. This relation eliminates the need to measure v_R, v_S and v_P independently: if two wave velocities are measured, the real roots of Eq. (4) determine the velocity of the third wave type.

2.1.2. Frequency domain: resonance

The resonant modes of a system are the result of interfering propagating waves. Mathematical models are readily available for regular systems such as solid spheres and cylinders, for example, where the first in depth study of vibrations of a homogeneous sphere was conducted by Lamb (1881). The normal modes of a solid sphere, determined by its radius and elastic properties (Snieder and Van Wijk, 2015), are separated into spheroidal S and torsional T modes. Each mode is characterized by their number of surface nodal lines l, number of internal nodal lines n, and azimuthal order m: ${}_nS_l^m$, and ${}_nT_l^m$. Here, we only consider the radial displacement of each mode, and because the torsional modes have no radial displacement these are omitted.

Spheroidal modes which have no internal nodal lines ($n=0$) are dominated by the constructive interference of surface Rayleigh waves (Stein and Wysession, 2009). Butkov (1968) shows that interfering Rayleigh waves which generate these modes have $\sqrt{l(l+1)}$ wavelengths on the surface of a sphere. Using this requirement it can be shown that the mode frequency ${}_nf_l$ for $n=0$ is related to the Rayleigh wave velocity and sphere radius R as

$${}_0f_l = \sqrt{l(l+1)}\frac{v_R}{2\pi R}, \tag{5}$$

where the Rayleigh wavelength is $\lambda_R = v_R/f_l$, R is the sphere radius and ${}_0f_l$ is the frequency of oscillation for ${}_0S_l^m$. Interference of surface Rayleigh waves with an oscillation frequency ${}_0f_l$ creates standing waves on the surface of the sphere. For an isotropic sphere, $2l+1$ modes exist at the same resonant frequency ${}_nf_l$, but have mode shapes based on the azimuthal order m. The magnitude of the surface displacement as a function of epicentral distance, θ, is governed by the associated Legendre polynomials

$$P_l^m(x) = \left[\frac{(1-x^2)^{m/2}}{2^l l!}\right]\left[\frac{d^{l+m}}{dx^{l+m}}(x^2-1)^l\right], \tag{6}$$

where $x = \cos\theta$ for a sphere.

Spheroidal modes which have no surface nodal lines ($l=0$), often termed radial modes, are dominated by the constructive interference of P-waves Aki and Richards (2002). The frequency of these modes can be found by finding the roots to:

$$\cot x = \frac{1}{x} - \frac{1}{4}\left(\frac{v_P}{v_S}\right)^2 x, \tag{7}$$

where

$$x = \frac{2\pi_n f_0 R}{v_P} \tag{8}$$

The lowest root of Eq. (7) corresponds to the fundamental mode ${}_0S_0^0$. The subsequent roots correspond to modes with $l=0$ and $n=1, 2, 3, \ldots$. For modes where both $n>0$ and $l>0$ there are no analytical solutions for the frequency of these modes, but a software package for seismology called Mineos (Masters et al., 2007) provides estimates of the eigen-frequencies of these modes.

2.1.3. Attenuation and quality factor

In the absence of damping, resonant modes are infinitely large in amplitude. However, internal friction (anelasticity) assures finite amplitude resonant peaks in the power spectrum. The quality factor Q is a measure of anelasticity (Vallina, 1999):

$$\frac{1}{Q(f)} = \frac{\delta f_l}{f_l}, \tag{9}$$

where f_l and δf_l are the center frequency and full width at half maximum of a resonance, respectively.

In the time domain, there is an equivalent contribution from anelasticity, as shown in Box 5.7 of Aki and Richards (2002):

$$A(t) = A_0\left(1-\frac{\pi}{Q(f)}\right)^{tf} \Leftrightarrow \ln(A(t)) = \ln(A_0) + tf\ln\left(1-\frac{\pi}{Q(f)}\right). \tag{10}$$

This means that the natural logarithm of the amplitude decay of propagating waves form a line with a slope defined by the quality factor $Q(f)$.

2.2. Non-contacting monitoring of a Braeburn apple

The Braeburn variety of apple is a firm eating apple with a spherical shape, of which the ripening process in modified atmospheres

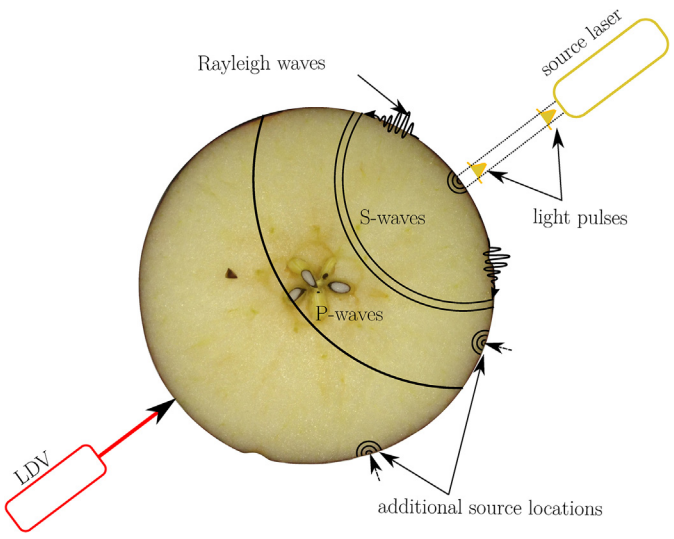

Fig. 1. Cross-section of an apple to illustrate that laser-generated elastic body- and surface-waves are detected with a laser Doppler vibrometer.

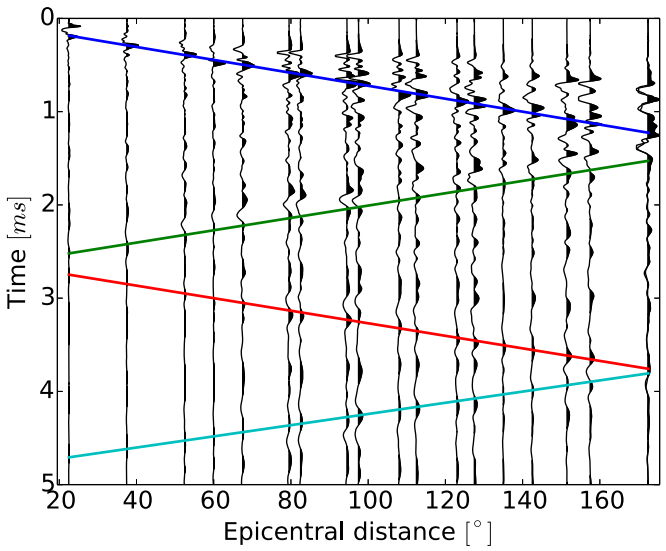

Fig. 2. Elastic wavefields as a function of time and angular distance around the apple reveal a wave speed of Rayleigh waves at $v_R = 100.5 \pm 0.1$ m/s.

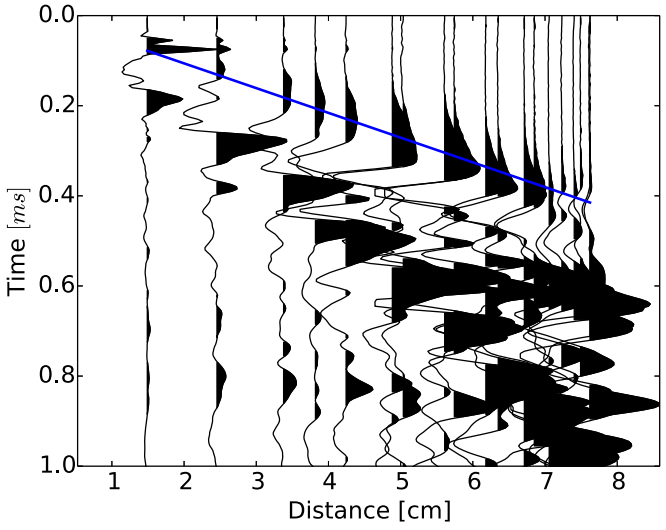

Fig. 3. Elastic wave fields as a function of time and the Euclidean distance through the apple from source to receiver. A linear regression on the primary wave arrival time results in a P-wave speed $v_P = 182 \pm 7$ m/s.

and internal browning has been studied extensively (Hertog et al., 2001; McGlone et al., 2005). We excite and detect elastic waves at a range of positions along the apple's equator to estimate the attenuation and elastic properties of a 189 g New Zealand Braeburn apple. Its density is 901 ± 1 kg/m^3 and the circumference is 24 cm, and the experiment was conducted under room conditions. The mass of the apple is measured with precision scales and the volume estimated from submersion in water.

2.2.1. Optical generation and detection of elastic waves

Elastic waves are generated optically to quantitatively estimate the elastic modulus E and the Poisson's ratio ν. Fig. 1 shows a cross section of the apple during excitation and the propagation paths of the generated surface and body elastic waves around the equator of the apple. A high energy laser pulse absorbed by the sample creates a localized area of rapidly increased temperature, and hence increased volume (i.e., thermo-elastic expansion), producing elastic waves (Scruby and Drain, 1990). Our source of elastic waves is a Quanta-Ray INDI pulsed laser with center wavelength of 1064 nm, pulse energy of 270 mJ, pulse duration of 10 ns, beam diameter of 4 mm, and a repetition rate of 10 Hz. We limit pulse energy and repetition rate of the laser to not damage the apple in the process. Both the surface and interior of the apple were visually assessed by cutting the apple along its equator, as shown in Fig. 1.

Elastic waves are detected using an optical heterodyne interferometer called a laser Doppler vibrometer (LDV). The LDV measures surface particle velocity (in mm/s) in the direction of the laser beam by detecting the Doppler shift of light backscattered by the sample (Scruby and Drain, 1990; Hitchman et al., 2015). LDVs have previously been used to detect the surface motion of fruit stimulated using a contacting source (Muramatsu et al., 2000; Terasaki et al., 2006). Excitation and detection of elastic waves using lasers offers several advantages over contacting transducer methods; namely the removal of source to sample coupling inconsistencies, small source and receiver footprint, and ease of scanning (Hitchman et al., 2015). A Polytec V505 LDV with V5000 demodulator was used to detect elastic waves. The LDV beam is focused to sub-millimeter diameter on the equator of the apple. LDV signal quality is aided by retro-reflective tape applied to the apple, but possibly could be removed with adequate signal processing and careful alignment of the apple and LDV. Data are recorded on an Alazar Tech digital oscilloscope card at 10^7 samples/s, and 16-bits dynamic range. Data acquisition is automated using the open-source Python control software PLACE (Johnson et al., 2015).

3. Results and discussion

3.1. The elastic properties

The wavefield as a function of time and distance (Fig. 2) is dominated by surface waves circling the apple multiple times. A band-pass filter with corner frequencies of 500 and 25,000 Hz was applied to remove high frequency noise of the detector and low frequency vibrations associated with rocking of the apple or remaining movement of the vibration-isolated optical bench. From the propagation of these surface waves, we estimate that the Rayleigh wave speed is $v_R = 100.5 \pm 0.1$ m/s. The earliest part of the same waveforms in Fig. 3 highlights the lower-amplitude arrival of the primary waves as a function of the distance through the flesh. A linear regression on this arrival results in a sub-sonic P-wave speed estimate $v_P = 182 \pm 7$ m/s.

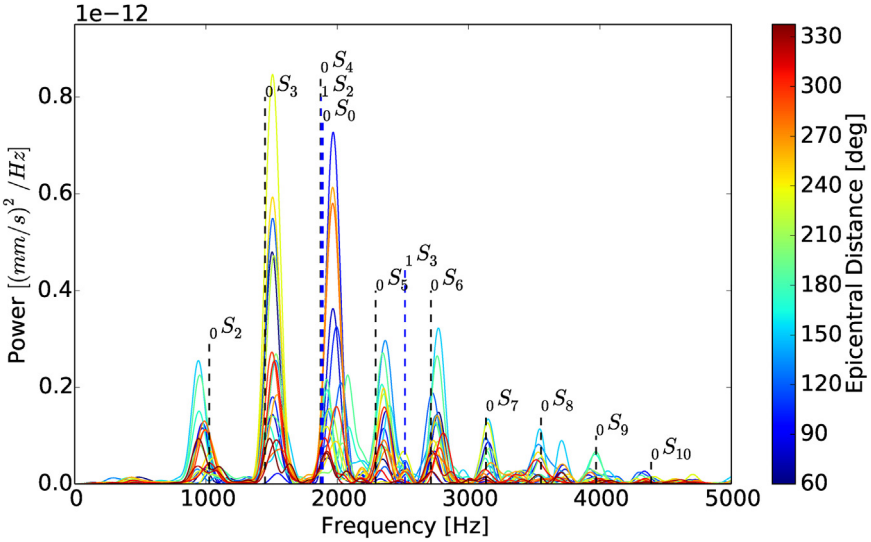

Fig. 4. The Power Spectral Density of the elastic wave fields from Fig. 2. The normal modes are identified with Eq. (5).

Due to limitations of typical LDVs, S-waves are not easily detected directly, unless a multi-component LDV is used (Blum et al., 2010). Instead, we calculate the shear wave velocity v_S from the P-wave and Rayleigh-wave speeds, and the real roots of Eq. (4), resulting in an estimate of $v_S = 110 \pm 4$ m/s. Eq. (3) shows that the elastic modulus and Poisson's ratio are related to the P- and S-wave velocities. Using Eq. (3) we find quantitative estimates of the elastic modulus $E = 26 \pm 1.5$ MPa, and Poisson's ratio $\nu = 0.21 \pm 0.05$.

3.1.1. *The normal modes of an apple*

Propagating elastic waves in the apple can be viewed as the superposition of its normal modes, as illustrated by the peaks in the Power Spectral Density (PSD) of the waveforms at all source-detector offsets (Fig. 4). Eqs. (5) and (7) and the Mineos code establishes which peak in the PSD corresponds to which spheroidal mode. In some cases, a peak in the PSD is close to many predicted modes. In such cases the dominant mode of a particular peak can be determined by the mode shape. Eq. (6) establishes the mode shape based on the azimuthal order m and surface nodal lines l. Experimentally we identify l and m of each spheroidal mode by plotting the peak power as a function of epicentral distance and compare to the predicted shape given by Eq. (6). The dominating lowest order modes were found using least square residuals to be $_0S_2^0$ (the so-called "breathing football" mode), $_0S_3^2$ and $_1S_2^0$ respectively, shown in Figs. 5 and 6 respectively. Finite element models for various apple shapes indicate that additional non-axisymmetric modes ($m \neq 0$) are stimulated with greater amplitudes relative to a sphere with similar elastic properties (Lu and Abbott, 1996). Resonant modes with $n = 0$ dominate the power spectra of the apple (Fig. 4), and are the result of interfering Rayleigh waves. Rayleigh surface waves experience 2-dimension geometric spreading, whereas body waves spread in three dimensions. Hence, it is not surprising that Rayleigh waves associated with $n = 0$ modes dominate over body-wave signals expressed in $n > 0$ overtones.

Tukey and Oran Young (1942) show that apple flesh is anisotropic at the cellular level due to cell elongation, air pockets and thickening of the cell wall during ripening. However, at these low frequencies the wavelengths in the apple are on the order of the size of the apple, and much greater than the cells. This means the isotropic model discussed in Section 2.1.2 allows us to explain our experiment.

The frequency of the $_0S_2^0$ mode, as shown in Fig. 4, closely matches previously presented values measured using contacting methods at comparable frequencies (Chen and DeBaerdemaeker, 1993; Yamamoto et al., 1980; Shmulevich et al., 2003) and has been

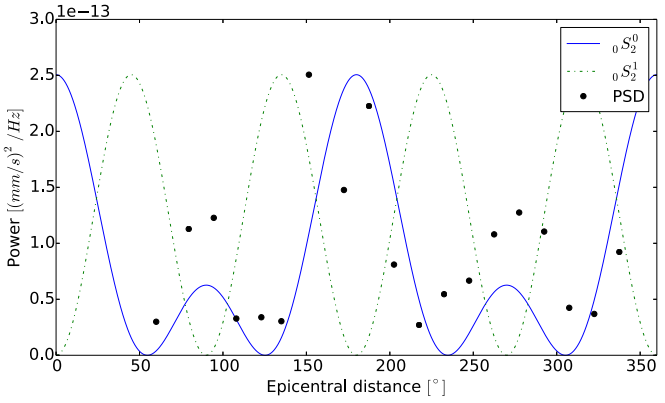

Fig. 5. The magnitude of the first mode as a function of epicentral distance (i.e., the distance between source and receiver) shows that the lowest order mode is dominated by the $_0S_2^0$ mode.

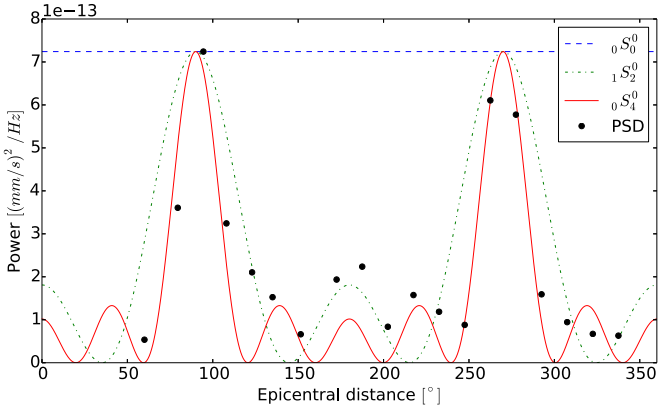

Fig. 6. The magnitude of the third mode as a function of epicentral distance (i.e., the distance between source and receiver) is dominated by the $_0S_4^0$ mode.

used to infer apple firmness via the Firmness Index (FI, Eq. (1)). The estimated elastic modulus $E = 26 \pm 1.5$ MPa, however, does not match previously reported measurements using compressive or destructive methods performed on apple flesh sections (Khan and Vincent, 1993; Varela et al., 2007), as these are performed at quasi-static conditions. The apple flesh is viscoelastic, and thus exhibits frequency dependence of its elastic properties (Varela et al., 2007). We further confirm our apple's viscoelasticity by examining the wave attenuation observed in its normal modes in the following section.

3.1.2. Normal mode quality factor

From the PSD of each waveform (Fig. 4), and Eq. (9), we estimate the quality factor Q for the lowest order modes ${}_0S_2$ and ${}_0S_3$ to be 7.7 ± 1.5 and 11.3 ± 1.6, respectively. Further Q estimates as a function of frequency for the waveform at 173° epicentral distance are termed Q_f in Fig. 4. The time-domain quality factor Q_t is estimated from Eq. (10) and the attenuation of all wave fields as a function of time. The quality factor Q in the apple generally increases with frequency, indicative of a viscoelastic medium (Fig. 7).

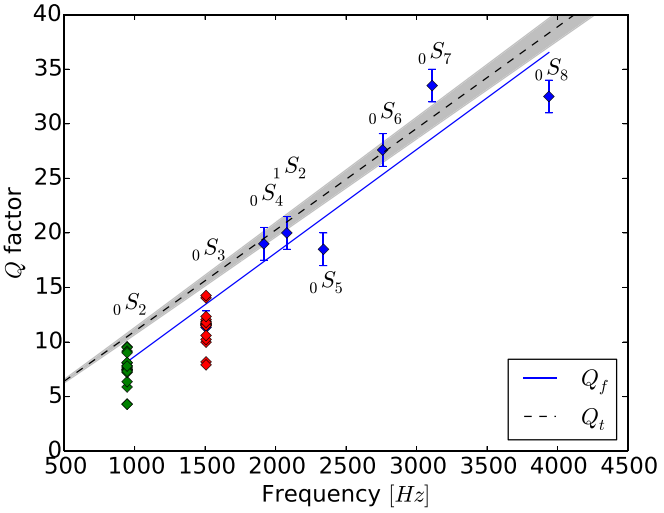

Fig. 7. The Q factor of the apple are estimated in both the frequency and time domain using Eq. (9) for Q_f and (10) for Q_t. We use the standard deviation of Q_f for the lowest order modes, ${}_0S_2$ and ${}_0S_3$, as the error in Q_f for higher order modes. The shaded area shows the error in Q_t based on a least squares regression of temporal attenuation of elastic waves.

3.2. Time lapse properties

Apple ripening results in softening flesh over time as cell structure breaks down, causing a dissolution of the cell wall and the middle lamella and growing intercellular spaces (Ben-Arie et al., 1979). Previous studies have shown that both elastic wave transmission and MT tests show a decrease in the elastic constants as apples mature (Chen et al., 1996). Our measurements on a single apple repeated daily for a period of fifteen days confirm this, and reveal that wave attenuation increases significantly with time. A control apple was placed in the same room conditions to monitor mass and volume throughout the experiment.

We estimate changes in the elastic and anelastic properties over 15 d from elastic waves recorded and detected daily at a source and receiver of 173°. Figs. 8 and 9 present the time-lapse elastic wave forms and their Power Spectral Density (PSD), respectively. Changes in the arrival time and amplitude of the elastic waves, as well as in the frequency of resonant modes indicate a decrease in the quality factor Q and the elastic moduli.

3.2.1. Elastic properties

The wave fields of Fig. 8 clearly show primary and surface waves arriving consistently later (and decreasing in amplitude). Fig. 8 shows that the P-wave arrival time increases at a rate of $\delta t_P = 3.96 \pm 0.07$ μs/d and the Rayleigh wave arrival time increases at a rate of $\delta t_R = 8.59 \pm 0.02$ μs/d. From these, we estimate that v_P and v_S decrease at a rate of $\delta v_P = -1.49 \pm 0.02$ m/s/d and $\delta v_S = -0.83 \pm 0.01$ m/s/d, respectively. Conversely, the resonant mode ${}_0S_2$ was found to decrease linearly at a rate of $\delta f = -9.4 \pm 0.2$ Hz/d.

The rate of change of the control apple density is estimated to be $\delta\rho = 820 \pm 50$ g/m^3/d. We extrapolate this gradient to the test apple and find that this linear increase in density fits within the error of initial and final density measurements of the test apple (see panel 1 of Fig. 10). From this, the estimated wave speeds, and Eq. (3), the elastic modulus and Poisson's ratio were estimated as the apple aged. A least-squares regression on the daily estimates of E in panel 2 of Fig. 10 indicates a decay rate of $\delta E = 0.355 \pm 0.005$ MPa/d, which amounts to a ~19% decrease over the fifteen day period. The Firmness Index FI (see panel 3 of Fig. 10) was calculated using the decay in the frequency of the ${}_0S_2$ mode, shown in Fig. 9, and the extrapolated apple mass using Eq. (1). Furthermore, a least-squares regression indicates a decay rate of the Firmness Index to be $\delta FI = 3336 \pm 3$ Hz^2/kg$^{2/3}$/d, which amounts to an overall decrease of ~30%. Finally, the Poisson's ratio (panel 4 of Fig. 10) does not decrease significantly, noting its relatively large standard

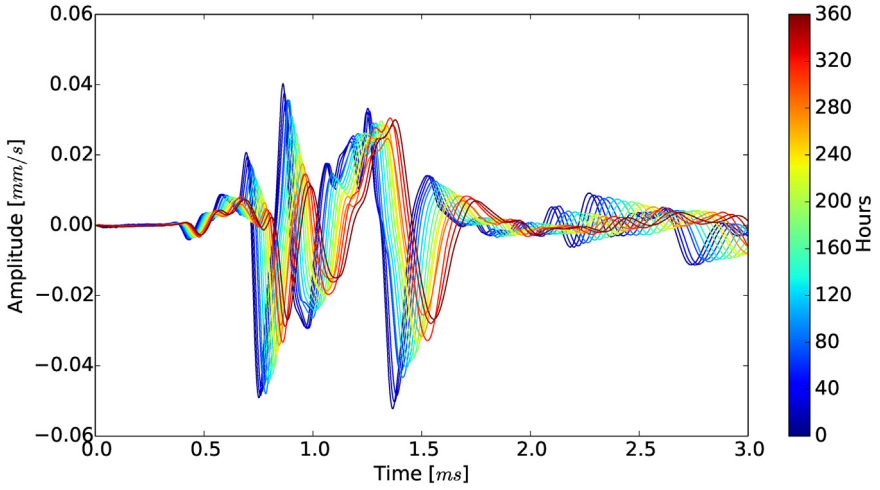

Fig. 8. Wave fields in the apple at a constant source-receiver epicentral distance of 173° indicate a decrease in velocity and an increase in attenuation over a period of 360 h.

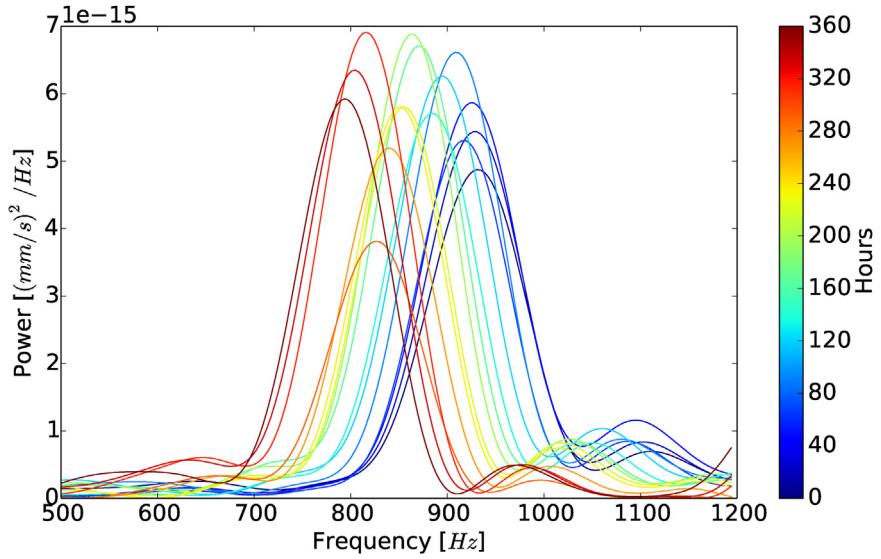

Fig. 9. The Power Spectral Density (PSD) of waves recorded at an epicentral distance of 173° display a decrease in the frequency of the first resonant mode, as the apple ages.

deviation. FI was found to decrease at a greater rate than the elastic modulus *E*. Eq. (2) reveals this difference can be attributed to changes in the primary wave speed decrease and the density increase.

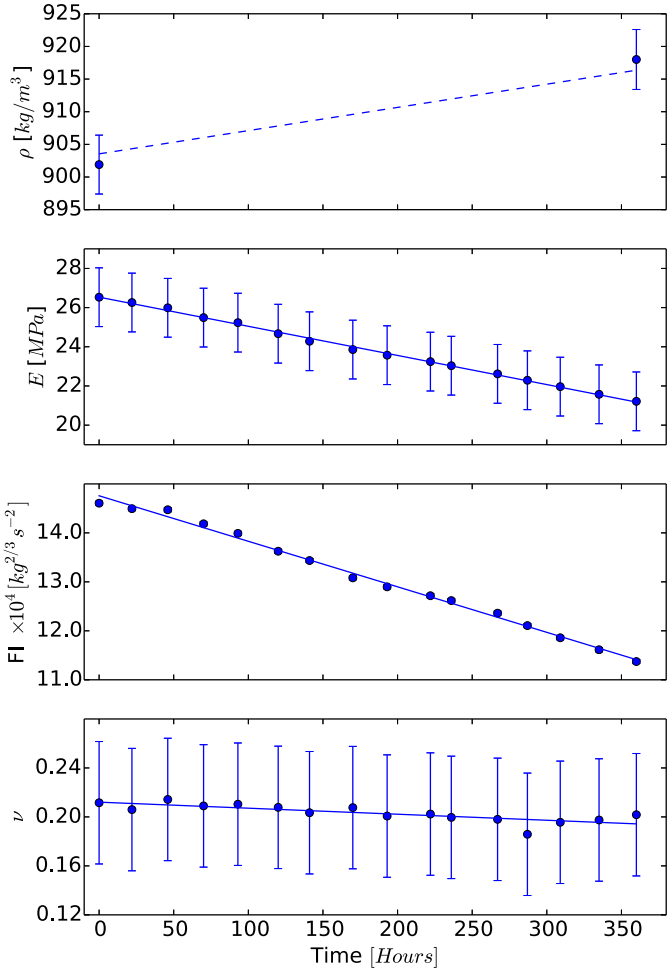

Fig. 10. Density, elastic modulus, FI, and Poisson's ratio estimated over a period of fifteen days. Error bars show the standard error in each property from initial measurements (Section 3).

3.2.2. Attenuation

The amplitude of the ${}_0S_2$ mode in Fig. 9 does not decay monotonically, and the estimated quality factor *Q* does not vary significantly, given our relatively large standard deviation on *Q* (top panel of Fig. 11). However, the amplitude of Rayleigh waves of Fig. 8 decay monotonically and significantly as the apple ages. Tracking the amplitude of the phase with the largest amplitude at $t = 0$ h, results in the bottom panel of Fig. 11. This amplitude decreases at a rate of $\delta A = 240 \pm 70$ nm/s/d, or 75% after 15 d. The Rayleigh wave amplitude was found to decrease at a significantly greater rate than the elastic constants or the FI, and may provide the most sensitive parameter of acoustic monitoring of the ripeness of an apple. However, Fig. 11 shows that the Q factor of the ${}_0S_2$ mode is approximately constant over the duration of this experiment. Therefore, in order to observe intrinsic absorption in the frequency domain, higher-order apple modes should be considered.

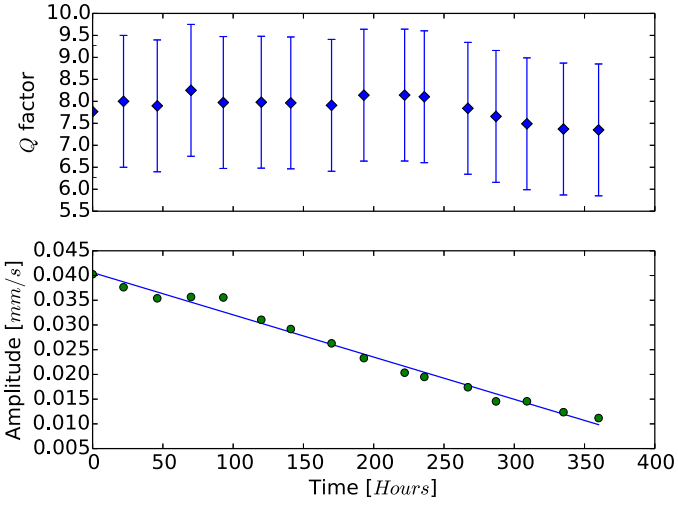

Fig. 11. The quality factor *Q* of the ${}_0S_2$ mode (top) and Rayleigh wave phase amplitude decay (bottom) measured as the apple ages. The error in *Q* is calculated using the standard deviation from the initial *Q* factor measurements on the ${}_0S_2$ mode (Fig. 7).

4. Conclusions

Fully non-contacting and non-destructive acoustic measurements on a Braeburn apple using laser ultrasound provide the means to monitor the ripeness with either propagating waves, or as the superposition of normal modes. A popular existing method to estimate the apple's (age-dependent) firmness – a quantity proportional to the elastic modulus – focuses on the fundamental mode of vibration. We find, however, that the elastic modulus decrease is less (19%) than the Firmness Index (30%) after fifteen days, and that the most sensitive parameter to monitor the ripeness of the apple is the attenuation of Rayleigh waves in the apple (75%). The Poisson's ratio and the quality factor Q of the fundamental mode of the apple were not found to decrease significantly over the same period. The introduced method of apple quality monitoring next needs to be tested on a range of apple (varieties) and to be made faster before it can be introduced in a commercial setting.

With these encouraging results by a new system to monitor the quality of a single apple, a study of a great variety of apples should be conducted next. Furthermore, to speed up the process we need to avoid the use of retro-reflective tape applied to the apple in future measurements. If successful, laser-ultrasonic monitoring may present an effective, non-contacting and non-destructive means of fruit and vegetable testing in a commercial setting.

References

Abbott, J.A., Bachman, G.S., Childers, R.F., Fitzgera, J.V., Matusik, F.J., 1968. Sonic techniques for measuring texture of fruits and vegetables. Food Technol. 22 (5), 101.

Abbott, J.A., Affeldt, H.A., Liljedahl, L.A., 1992. Firmness measurement of stored delicious' apples by sensory methods, Magness–Taylor, and sonic transmission. J. Am. Soc. Horticult. Sci. 117 (4), 590–595.

Adam, L., Ou, F., Strachan, L., Johnson, J., van Wijk, K., Field, B., 2014. Mudstone P-wave anisotropy measurements with non-contacting lasers under confining pressure. In: SEG Technical Program Expanded Abstracts.

Aki, K., Richards, P.G., 2002. Quantitative Seismology, 2nd ed. University Science Books.

Ben-Arie, R., Kislev, N., Frenkel, C., 1979. Ultrastructural changes in the cell walls of ripening apple and pear fruit. Plant Physiol. 64 (2), 197–202.

Blum, T.E., van Wijk, K., Pouet, B., Wartelle, A., 2010. Multicomponent wavefield characterization with a novel scanning laser interferometer. Rev. Sci. Instrum. 81, 073101.

Blum, T.E., Adam, L., van Wijk, K., 2013. Noncontacting benchtop measurements of the elastic properties of shales. Geophysics 78 (3), C25–C31.

Butkov, E., 1968. Mathematical Physics. Addison-Wesley Series in Advanced Physics.

Chen, H., DeBaerdemaeker, J., 1993. Effect of apple shape on acoustic measurements of firmness. J. Agric. Eng. Res. 56 (3), 253–266.

Chen, H., Duprat, F., Grotte, M., Loonis, D., Pietri, E., 1996. Relationship of impact transmission wave to apple texture during ripening. J. Texture Stud. 27 (2), 123–141.

Cooke, J.R., Rand, R.H., 1973. A mathematical study of resonance in intact fruits and vegetables using a 3-media elastic sphere model. J. Agric. Eng. Res. 18 (2), 141–157.

Duprat, F., Grotte, M., Pietri, E., Loonis, D., Studman, C.J., 1997. The acoustic impulse response method for measuring the overall firmness of fruit. J. Agric. Eng. Res. 66 (4), 251–259.

Hertog, M.L.A.T.M., Nicholson, S.E., Banks, N.H., 2001. The effect of modified atmospheres on the rate of firmness change in Braeburn apples. Postharvest Biol. Technol. 23 (3), 175–184.

Hitchman Sam, van Wijk Kasper, Broderick Neil, Adam Ludmila, 2015. Heterodyne interferometry for the detection of elastic waves: a tutorial and open-hardware project. Eur. J. Phys. 36 (3), 035011.

Huang, M., Lu, R., 2010. Apple mealiness detection using hyperspectral scattering technique. Postharvest Biol. Technol. 58 (3), 168–175, http://dx.doi.org/10.1016/j.postharvbio.2010.08.002, ISSN: 0925-5214. http://www.sciencedirect.com/science/article/pii/S0925521410001766.

Ikeda, T., Choi, P.-K., Ishii, T., Arai, I., Osawa, M., 2015. Firmness evaluation of watermelon flesh by using surface elastic waves. J. Food Eng. 160, 28–33.

Johnson, J.L., van Wijk, K., Sabick, M., 2014. Characterizing phantom arteries with multi-channel laser ultrasonics and photo-acoustics. Ultrasound Med. Biol. 40 (3), 513–520.

Johnson, J.L., tom, W.H., van Wijk, K., 2015. PLACE an open-source python package for laboratory automation, control, and experimentation. J. Lab. Autom. 20 (1), 10–16.

Khan, A.A., Vincent, J.F.V., 1993. Compressive stiffness and fracture properties of apple and potato parenchyma. J. Texture Stud. 24 (4), 423–435, http://dx.doi.org/10.1111/j.1745-4603.1993.tb00052.x, ISSN: 1745-4603.

Lamb, H., 1881. On the vibrations of an elastic sphere. Proc. London Math. Soc. s1-13 (1), 189–212, http://dx.doi.org/10.1112/plms/s1-13.1.189.

Lu, R., Abbott, J.A., 1996. Finite element analysis of modes of vibration in apples. J. Texture Stud. 27 (3), 265–286.

Lu, R., Peng, Y., 2006. Hyperspectral scattering for assessing peach fruit firmness. Biosyst. Eng. 93 (2), 161–171, http://dx.doi.org/10.1016/j.biosystemseng.2005.11.004, ISSN: 1537-5110. http://www.sciencedirect.com/science/article/pii/S1537511005002552.

Magness, J.R., Taylor, G.E., 1925. Improved type of pressure tester for the determination of fruit maturity. In: Circulation No. 350.

Masters, G., Barmine, M.P., Kientz, S., 2007. Mineos user's manual. Comput. Infrastruct. Geodyn.

McGlone, A.V., Martinsen, P.J., Clark, C.J., Jordan, R.B., 2005. On-line detection of Brownheart in Braeburn apples using near infrared transmission measurements. Postharvest Biol. Technol. 37 (2), 142–151.

Muramatsu, N., Sakurai, N., Wada, N., Yamamoto, R., Tanaka, K., Asakura, T., Ishikawa-Takano, Y., Nevins, D.J., 2000. Remote sensing of fruit textural changes with a laser Doppler vibrometer. J. Am. Soc. Horticult. Sci. 125 (1), 120–127.

Peng, Y., Lu, R., 2007. Prediction of apple fruit firmness and soluble solids content using characteristics of multispectral scattering images. J. Food Eng. 82 (2), 142–152, http://dx.doi.org/10.1016/j.jfoodeng.2006.12.027, ISSN: 0260-8774. http://www.sciencedirect.com/science/article/pii/S0260877407000702.

Rayleigh, L., 1885. On waves propagated along the plane surface of an elastic solid. Proc. London Math. Soc. s1-17 (1), 4–11, http://dx.doi.org/10.1112/plms/s1-17.1.4.

Scruby, C.B., Drain, L.E., 1990. Laser Ultrasonics: Techniques and Applications. Adam Hilger.

Shmulevich, I., Galili, N., Howarth, M.S., 2003. Nondestructive dynamic testing of apples for firmness evaluation. Postharvest Biol. Technol. 29 (3), 287–299, http://dx.doi.org/10.1016/S0925-5214(03)00039-5, ISSN: 0925-5214. http://www.sciencedirect.com/science/article/pii/S0925521403000395.

Snieder, R., Van Wijk, K., 2015. A Guided Tour of Mathematical Methods for the Physical Sciences, 3rd ed. Cambridge University Press.

Stein, S., Wysession, M., 2009. An Introduction to Seismology, Earthquakes, and Earth Structure. John Wiley & Sons.

Terasaki, S., Sakurai, N., Zebrowski, J., Murayama, H., Yamamoto, R., Nevins, D.J., 2006. Laser Doppler vibrometer analysis of changes in elastic properties of ripening 'la France' pears after postharvest storage. Postharvest Biol. Technol. 42 (2), 198–207.

Tukey, H.B., Oran Young, J., 1942. Gross morphology and histology of developing fruit of the apple. Bot. Gazet. 104 (1), 3–25, ISSN: 00068071. http://www.jstor.org/stable/2471996.

Vallina, A.U., 1999. Principles of Seismology. Cambridge University Press.

Varela, P., Salvador, A., Fiszman, S., 2007. Changes in apple tissue with storage time: rheological, textural and microstructural analyses. J. Food Eng. 78 (2), 622–629, http://dx.doi.org/10.1016/j.jfoodeng.2005.10.034, ISSN: 0260-8774. http://www.sciencedirect.com/science/article/pii/S0260877405007478.

Yamamoto, H., Iwamoto, M., Haginuma, S., 1980. Acoustic impulse response method for measuring natural frequency of intact fruits and preliminary applications to internal quality evaluation of apples and watermelons. J. Texture Stud. 11 (2), 117–136, http://dx.doi.org/10.1111/j.1745-4603.1980.tb00312.x, 6. ISSN: 1745-4603.

Zhang, W., Cui, D., Ying, Y., 2014. Nondestructive measurement of pear texture by acoustic vibration method. Postharvest Biol. Technol. 96, 99–105, http://dx.doi.org/10.1016/j.postharvbio.2014.05.006, ISSN: 0925-5214. http://www.sciencedirect.com/science/article/pii/S092552141400132X.